Alzheimer's & Dementia: Diagnosis, Assessment & Disease Monitoring 11 (2019) 576-587

Neuroimaging

White matter alterations in early-stage Alzheimer's disease: A tract-specific study

Qiuting Wen[a,b], Sourajit M. Mustafi[a,b], Junjie Li[c], Shannon L. Risacher[a,b], Eileen Tallman[a,b], Steven A. Brown[d], John D. West[a,b], Jaroslaw Harezlak[e], Martin R. Farlow[b,f], Frederick W. Unverzagt[b,g], Sujuan Gao[d], Liana G. Apostolova[a,b,f], Andrew J. Saykin[a,b,f,g], Yu-Chien Wu[a,b,*]

[a]*Department of Radiology and Imaging Sciences, Indiana University School of Medicine, Indianapolis, IN, USA*
[b]*Indiana Alzheimer Disease Center, Indiana University School of Medicine, Indianapolis, IN, USA*
[c]*University Information Technology Service - Research Technology, Indiana University, Indianapolis, IN, USA*
[d]*Department of Biostatistics, Indiana University School of Medicine, Indianapolis, IN, USA*
[e]*Department of Epidemiology and Biostatistics, School of Public Health, Indiana University, Bloomington, IN, USA*
[f]*Department of Neurology, Indiana University School of Medicine, Indianapolis, IN, USA*
[g]*Department of Psychiatry, Indiana University School of Medicine, Indianapolis, IN, USA*

Abstract

Introduction: Diffusion magnetic resonance imaging may allow for microscopic characterization of white matter degeneration in early stages of Alzheimer's disease.

Methods: Multishell Diffusion magnetic resonance imaging data were acquired from 100 participants (40 cognitively normal, 38 with subjective cognitive decline, and 22 with mild cognitive impairment [MCI]). White matter microscopic degeneration in 27 major tracts of interest was assessed using diffusion tensor imaging (DTI), neurite orientation dispersion and density imaging, and q-space imaging.

Results: Lower DTI fractional anisotropy and higher radial diffusivity were observed in the cingulum, thalamic radiation, and forceps major of participants with MCI. These tracts of interest also had the highest predictive power to discriminate groups. Diffusion metrics were associated with cognitive performance, particularly Rey Auditory Verbal Learning Test immediate recall, with the highest association observed in participants with MCI.

Discussion: While DTI was the most sensitive, neurite orientation dispersion and density imaging and q-space imaging complementarily characterized reduced axonal density accompanied with dispersed and less restricted white matter microstructures.

Keywords: Alzheimer's disease; Magnetic resonance imaging; Diffusion imaging; White matter; Tract; Tractography; diffusion tensor imaging; NODDI; SCD; MCI

1. Introduction

Alzheimer's disease (AD)-associated changes in the brain begin decades before symptoms become evident [1,2]. The long presymptomatic stage of AD provides a valuable window for early intervention with disease-modifying therapy if the mechanisms of AD can be detected using reliable biomarkers. Among neuroimaging biomarkers, magnetic resonance imaging (MRI) is a safe, noninvasive, and nonradiating technique suitable for preclinical screening and monitoring disease progression in AD. Volumetric

*Corresponding author. Tel.: +317-963-1697; Fax: +317-963-7547.
E-mail address: yucwu@iu.edu

https://doi.org/10.1016/j.dadm.2019.06.003

measurements using T1-weighted MRI are used extensively to detect AD and other dementia-associated brain atrophy, which could include a combination of microscopic degenerative processes, such as neuronal death, myelin degeneration, and loss of neurites or axons [3–5]. Such microscopic alterations may be assessed by diffusion MRI (dMRI), an imaging method for probing human brain microstructures.

Diffusion MRI provides imaging metrics of the cellular organization by measuring water diffusion properties under the influence or restriction of biological barriers. Cellular microarchitectures create restricted environments that shape the diffusion probability function of water molecules. Therefore, the shape, size, and properties of the diffusion function estimated by dMRI allow for quantitative assessment of AD-associated microscopic degeneration. For example, diffusion tensor imaging (DTI) produces two summary metrics, fractional anisotropy (FA) and mean diffusivity (MD), and two orthogonal metrics, axial diffusivity (Da) and radial diffusivity (Dr). FA, the variance of Da and Dr, indicates how elongated the diffusion is and reflects the coherence of underlying tissue or the fiber organization. MD, the mean diffusion in three directions, describes the general freedom of diffusion in the tissue regardless of the directionality. FA and MD have been the main focus in DTI studies of AD, whereas Da and Dr, associated with axonal and myelin integrity in animal studies [6], may help to interpret potential neurobiological mechanisms [7].

DTI is sensitive to white matter degeneration in the early stages of AD, including in subjective cognitive decline (SCD), a potential preclinical stage of AD [8–11], and amnestic mild cognitive impairment (MCI), a prodromal stage of AD [8,12–17]. Diffusion metrics in SCD have been shown to be intermediate between cognitively normal (CN) older adults and individuals with MCI [8,9,11]. Across the disease continuum, the direction of changes in DTI metrics are as follows: (1) decreased FA, indicating loss of tissue organization and/or (2) increased mean and radial diffusivities, suggesting a breakdown of neurobiological barriers (myelin degeneration or cell membrane deterioration) or cytotoxic edema [8,9,11–16].

In addition to classic DTI approaches, a recent advance in dMRI is the ability to assess axonal density and cellularity among other microstructural features [18–21]. Diffusion microstructural features are obtained through nonparametric q-space analyses and parametric compartment modeling. The q-space analyses provide a metric for tissue restriction (P_0) associated with myelination in animal studies of dysmyelination [22,23] and in human studies of multiple sclerosis [24] and aging [25]. Parametric diffusion modeling further decodes the diffusion signal into multiple compartments (e.g., extracellular and intracellular) and provides neurobiological metrics. Since 1997, many diffusion models have been proposed and applied to animal [26,27] and human studies [18–20]. One of the diffusion compartment models, called neurite orientation dispersion and density imaging (NODDI), proposed that white matter tissue comprises three diffusion compartments detectable by using modern clinical MRI scanners with a reasonable scan time [20]. The NODDI approach provides the intra-axonal volume fraction (ICVF) as a proxy for axonal density and an orientation dispersion index that describes the axonal organization. While DTI provides a general assessment of averaged microstructures within an imaging voxel, NODDI provides diffusion metrics with a finer granularity that further decipher intracellular and extracellular microscopic properties. We believe that the NODDI-derived axonal density may provide explanation and details on potential disease mechanisms of why and how changes in the AD white matter were observed by DTI.

The NODDI approach has been validated with histologic evidence reported in the literature. The NODDI-derived axonal density (ICVF) is almost identical to values obtained from electron microscopy of *ex vivo* mouse brain and in good agreement with previously reported fiber densities of the human brain obtained by electron microscopy [28]. In addition, ICVF correlates with an animal model of tau pathology in AD [29]. *In vivo* applications suggest that NODDI can detect white matter changes in the aging brain [25,30–33], and associations of NODDI-derived metrics with focal cognitive deficits and the APOEε4 status in young-onset AD have been demonstrated [34].

Here, we used complementary diffusion metrics (i.e., DTI, NODDI, and q-space) to study white matter alterations in early-stage AD. We focused on individuals with objective cognitive impairment (MCI) and individuals with only SCD assessed via the Cognitive Change Index (CCI), a comprehensive measure of perceived neuropsychological function focusing on the memory, executive, and language domains [35,36]. To investigate AD-related anatomical variations, we performed tract-specific analyses focusing on 27 major white matter bundles across the entire brain. The tracts of interest were generated by crossing fiber model–based probability tractography rendered by a coregistered white matter atlas [37]. This study identified the best diffusion-anatomical classifiers and their associations with clinical outcomes. We hypothesized that besides commonly reported hippocampal fiber tracts (e.g., limbic system), additional white matter fiber tracts outside the limbic system can significantly differentiate cognitive impairment and that the deteriorations in these fiber tracts are associated with neuropsychological assessment scores.

2. Methods

2.1. Participants

Indiana Alzheimer's Disease Center (IADC) funded by NIA P30s since 1991 has screened approximately 2000 subjects and created an extensive longitudinal clinical database. In 2008, the Neuroimaging Core was added, and it recruits approximately 50-100 subjects per year to be available for

neuroimaging studies. An advanced multishell diffusion imaging technique, hybrid diffusion imaging (HYDI), was added to the IADC routine MRI protocol in April 2015. All IADC participants received the Uniform Data Set version 3 battery (as used in all NIA AD Centers) [38] and additional neuropsychological tests used at the IADC with special emphasis on memory and executive function (see details in the Neuropsychological Assessment section). Exclusion criteria for neuroimaging were significant cerebrovascular disease or malformations; a history of chemotherapy or radiation therapy; current major depression; a history of schizophrenia, bipolar disorder, developmental disability, Parkinson disease, brain surgery, brain infection, or significant head injury (loss of consciousness $>$ 30 min); and/or excessive alcohol consumption. All participants provided written informed consent according to procedures approved by the Institutional Committee for the Protection of Human Subjects at Indiana University School of Medicine (IRB no.: 1604443276).

IADC participants who received HYDI were included in the study. No other specific selection or screening on the IADC participants were performed. By the time of data processing for the study in 2017, there were 100 participants who had HYDI scans. Among them, 40 were CN, 38 had SCD, and 22 had amnestic MCI. The data on age, sex, education level, and diagnoses for the subjects were extracted from their annual clinical assessments in the same year of the HYDI scans.

2.2. Clinical and neuropsychological assessment

Participants were evaluated using a detailed neuropsychological battery, including measures of memory, attention, executive function, language, visuospatial ability, general intellectual ability, and psychomotor speed. These psychological tests included the Rey Auditory Verbal Learning Test (RAVLT), the Montreal Cognitive Assessment (MoCA) for dementia severity [39], Clinical Dementia Rating sum of boxes (CDR-SB) [40], the 15-item Geriatric Depression Scale (score was calculated removing the item asking about memory issues) (adjusted Geriatric Depression Scale [GDS]) [41], and the CCI to evaluate self-reported SCD [36]. Additional items listed in Uniform Data Set version 3 were also administrated including: Craft Story 21, Benson complex figure copy and recall, number span test, multilingual naming test (MINT), phonemic test, animal and vegetable list generation, and Trail Making Test (executive function) [38].

Group classifications (CN, SCD, MCI) were based on the neuropsychological assessment by two board-certified neurologists (L.G.A. and M.R.F.) and two neuropsychologists (F.W.U. and A.J.S.). Subjects with amnestic MCI were identified based on the National Institute on Aging-Alzheimer's Association criteria [42] with objective education-adjusted memory or other cognitive impairment and a global CDR of 0.5. The subjects with SCD were subsequently identified from CN subjects if their self-reported CCI score on the first 12 memory items was $\geq$20 [36,43]. Psychological tests scores included in this study to associate with imaging findings were the RAVLT immediate recall (RAVLT-IR) and delayed recall (RAVLT-DR), MoCA, CDR-SB, adjusted GDS, and CCI.

2.3. MRI acquisition

All brain MRIs were performed on a single Siemens Prisma 3T scanner with standard Siemens 64-channel RF receiver head coil. All subjects received anatomical T1-weighted and T2-weighted fluid-attenuated inversion recovery (FLAIR) imaging and dMRI. The imaging sequences and parameters of the anatomical scans followed the Alzheimer's Disease Neuroimaging Initiative 2 protocols (http://adni.loni.usc.edu/methods/documents/mri-protocols/) and were reviewed by neuroradiologists for incidental findings.

The dMRI protocol used a single-shot spin-echo echo-planar imaging sequence with a HYDI scheme that contained three zero diffusion-weighting (i.e., b-value = 0 s/mm^2) and five concentric diffusion-weighting shells (b-values = 0, 250, 1000, 2000, 3250, 5000 s/mm^2) with 142 diffusion-weighting gradient directions [44]. The field of view was 240 $\times$ 240 mm with an imaging matrix of 120 $\times$ 120 and 68 slices of 2-mm slice thickness, yielding 2-mm isotropic voxels. An additional b = 0s/mm^2 with reversed-phase encoding was acquired for geometric distortion correction.

2.4. Diffusion image processing, model fitting, and tractography

Image processing included preprocessing followed by computation of diffusion metrics and tractography. The diffusion-weighted images were first denoised using the local principal component analysis approach [45]. With a pair of reverse phase–encoded b0 images as reference, the denoised diffusion-weighted images were corrected for static-field geometric distortion, motion, eddy current artifacts using the TOPUP and EDDY tool from FMRIB software library (FSL) (http://fsl.fmrib.ox.ac.uk/fsl).

The preprocessed HYDI data were used to compute diffusion metrics of DTI, NODDI, and q-space imaging [25]. The DTI metrics were computed using the FSL DTIFIT command on the first (b-value = 250 s/mm^2) and second shells (b-value = 1000 s/mm^2) of the HYDI data, including FA (the coherence of microstructure water diffusion), MD (the magnitude of overall water diffusion), and supplementary analyses of axial (Da, along the principal water diffusion direction) and Dr (perpendicular to the principal water diffusion direction). All five HYDI shells were used in the NODDI analysis with the AMICO toolbox (https://github.com/daducci/AMICO) [46]. Unlike the classic diffusion tensor model, the NODDI model proposes specific assumptions about the way in which local microarchitecture affects the diffusion properties. In particular, it models the water

diffusion signal according to one of three different pools: (1) free-water diffusion (such as in cerebrospinal fluid); (2) intracellular restricted diffusion inside dendrites and axons, and (3) extracellular hindered diffusion. The resultant indices included in the analysis are the ICVF, a measure of neurite density, and neurite orientation dispersion index (OD, the degree of fanning in neurite orientation). In addition to DTI and NODDI, zero-displacement probability (P_0) was estimated by integrating the volume of the q-space signals, which reflects water mobility or tissue restrictions. This q-space approach is model free, as it does not use any assumptions of the underlying diffusion properties [44]. Supplementary Table 1 summarizes the diffusion metric acronyms and their microstructure implications.

Parallel to metrics fitting, a within-voxel multifiber tract orientation structure was modeled using BEDPOSTx followed by probabilistic tractography (with crossing fiber modeling [47]) using PROBTRACKx [48]. For each subject, automatic mapping of the 27 major white matter tracts was conducted in the native diffusion space. The start/stop region-of-interest masks of the 27 major white matter bundles were first rendered and identified in a coregistered standard Montreal Neurological Institute space before being reversely transformed to the native diffusion space (as implemented in the AutoPtx plugin for FSL) [37]. Tract-specific measures of diffusion metrics (i.e., FA, MD, Da, Dr, ICVF, OD, P_0) were derived for the following 27 tracts of interest [49]: middle cerebellar peduncle (mcp); medial lemniscus (ml); uncinate fasciculus (unc); cingulate gyrus and parahippocampal portions of the cingulum bundle (cgc, cgh); forceps major and minor (fma, fmi); corticospinal tract (cst); acoustic radiation (ar); anterior, superior, and posterior thalamic radiation (atr, str, ptr); and superior, inferior longitudinal, and inferior fronto-occipital fasciculi (slf, ilf, ifo) (Fig. 1).

2.5. Statistical analysis

Statistical analyses were conducted using R-3.3.3. For demographic and cognitive variables comparisons, analyses of variance (ANOVA) were used. For the diffusion variables, between-group analyses were performed using two approaches. First, we examined overall group differences among the three groups using F-tests, followed by ANOVA tests for pair-wise group differences. Bonferroni correction was used to adjust the *P* value for multiple comparisons

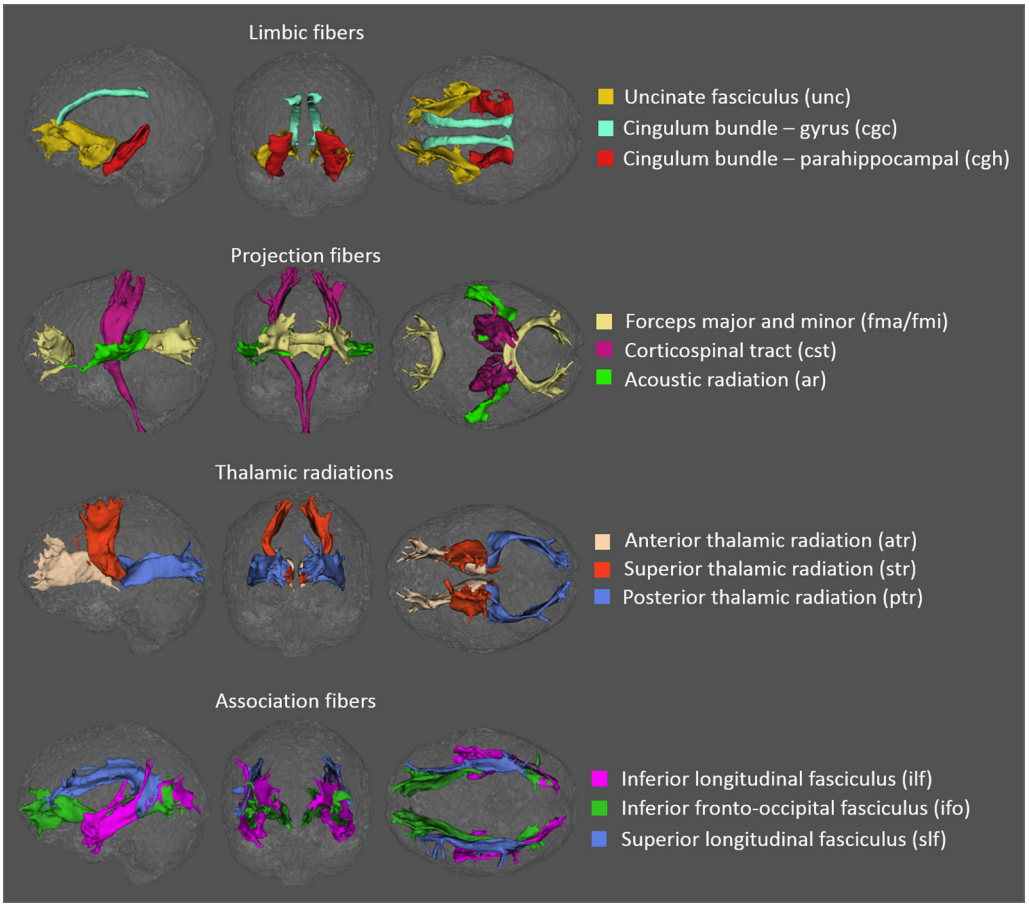

Fig. 1. White matter tracts of interest in one cognitively normal subject generated using probabilistic tractography rendered in sagittal (left), coronal (center), and axial (right) views. The 27 tracts of interest were grouped into five categories: the brainstem (not shown here), limbic fibers connecting the limbic system (first row), projection fibers (second row), thalamic radiations (third row), and association fibers (fourth row).

among all 27 tracts of interest for each diffusion parameter. Second, we studied which combination of diffusion metrics within tract of interests can best classify the disease stage. To do so, we used an extension of the regularization approach called least absolute shrinkage and selection operator (LASSO) [50]. The classification was performed via the penalized logistic regression using the function glmnet (an R library "glmnet"). To select the optimal predictors in the training phase, we run 100 iterations. In each iteration, predictors that gave a cross-validated error within one standard error of the minimum were selected. The predictors that appeared in the majority of the iterations (greater than 50%) were entered into the prediction phase. The final prediction and receiver operating characteristic curves were obtained using a prediction method with a general linear model. Linear regression was used to assess the relationships between neuropsychological performance and diffusion variables on tracts identified in the LASSO analysis.

To identify the best-correlated pairs between neuropsychological scores and diffusion variables, sparse canonical correlation analysis was performed (function "CCA" in R library "PMA"). Briefly, permutation analysis was performed to produce the optimal tuning parameters for sparse canonical correlation using the penalized matrix decomposition using the R function "*CCA.permute*". Afterward, sparse canonical correlations were applied with the optimal tuning parameters to produce the most correlated pair(s) between the diffusion metrics and neuropsychological measures using the R function "*CCA*". All regression analyses mentioned previously were controlled for age, sex, and education level. The LASSO and CCA approaches inherently account for multiple comparisons.

3. Results

3.1. Subject characteristics and clinical outcomes

The three groups of participants did not differ significantly with respect to age, sex, or education level ($ps > 0.05$, Table 1). As expected by design, the subjects with MCI demonstrated significantly worse cognitive function, including lower RAVLT-IR, RAVLT-DR, and MoCA and higher CDR-SB scores ($ps < 0.001$). Compared with the CN group, the SCD group had a higher CCI by design ($ps < .001$), but did not differ in objective neuropsychological test scores, including the RAVLT-IR, RAVLT-DR, MoCA, and CDR ($ps > 0.05$). While the adjusted GDS scores of all subjects were normal and below the clinical cutoff for depression (i.e., >9), the MCI and SCD groups had higher GDS scores than the CN group ($ps < 0.05$).

3.2. Tract characteristics and group-wise differences

In Supplementary Fig. 1, tract-specific values for each of the diffusion parameters (i.e., FA, MD, Da, Dr, ICVF, OD, and P_0) are displayed as boxplots by group. Among the 27 tracts of interest, the forceps major (fma) had the highest FA and lowest OD, as expected. The high FA in the forceps major was mostly driven by high Da with relatively low Dr. The bilateral parahippocampal cingulum (cgh) had the lowest FA and highest OD, which was driven by high Dr. Also, the bilateral parahippocampal cingulum (cgh) had the lowest neurite density (ICVF) and the lowest tissue restriction (P_0). In most tracts, the SCD group demonstrated diffusion values that were intermediate between those of the CN and MCI groups.

Following the F-tests for overall group effects (Supplementary Table 2), tract-specific diffusion values were evaluated by ANOVA to examine between-group differences (Supplementary Fig. 2A, before Bonferroni correction). In general, the MCI group had a relatively lower coherence of water diffusion (decreased FA and increased dispersion, OD), neurite density (ICVF), and tissue restriction (P_0), but a relatively higher magnitude of water diffusion (MD, Da, and Dr) across the tracts of interest. Compared with the CN, the SCD group had lower Da in

Table 1
Subject characteristics and cognitive function

	CN	SCD	MCI		Post-hoc comparison			
Characteristic	n = 40	n = 38	n = 22	*P* value	CN-SCD	SCD-MCI	CN-MCI	*N*
Age (yrs)	68.3 (6.3)	68.7 (8.9)	72.2 (10.3)	.18	0.98	0.26	0.19	40/38/22
Sex (M:F)	8:32	12:26	9:13	.21	0.5	0.72	0.2	40/38/22
Education (yrs)	16.4 (2.6)	16.5 (2.5)	16.5 (2.7)	.99	0.99	1	0.99	40/38/22
CCI	15.3 (2.1)	27.4 (6.3)	32.7 (10.9)	<.001	<0.001	0.011	<0.001	40/38/19
RAVLT-IR	47.7 (8.3)	46 (8.3)	32.9 (7.7)	<.001	0.66	<0.001	<0.001	34/37/18
RAVLT-DR	9.7 (2.8)	9.8 (2.9)	3.1 (2.7)	<.001	1	<0.001	<0.001	34/37/19
MoCA	26.6 (2.2)	26.2 (2.6)	21.5 (3.5)	<.001	0.84	<0.001	<0.001	40/38/21
CDR	0.1 (0.3)	0.1 (0.3)	1.7 (1.3)	<.001	0.99	<0.001	<0.001	40/38/22
Adjusted GDS	0.5 (0.8)	1.8 (2.1)	2.5 (3)	<.001	0.014	0.38	<0.001	40/38/22

NOTE. Demographic and cognitive characteristics include mean (standard deviation) for each group.

Abbreviations: CN, cognitively normal; SCD, subjective cognitive decline; MCI, mild cognitive impairment; CCI, Cognitive Change Index; RAVLT-IR, Rey Auditory Verbal Learning Test immediate recall (sum score of initial five learning trials); RAVLT-DR, Rey Auditory Verbal Learning Test delayed recall; MoCA, Montreal Cognitive Assessment; CDR, Clinical Dementia Rating; and adjusted GDS, Geriatric Depression Scale without the cognitive item.

the forceps major (fma) and left superior longitudinal fasciculus (slf).

With the Bonferroni correction (Supplementary Fig. 2B and Fig. 2A), a subset of tracts in MCI with significant differences relative to CN or SCD emerged, including the parahippocampal cingulum (cgh), posterior thalamic radiation (ptr), forceps major (fma), and inferior fronto-occipital fasciculi (ifo). Dr was significantly higher in MCI, whereas Da was not (Fig. 2A. Consequently, FA was lower and MD was higher in the MCI group relative to the CN or SCD group. Tracts exhibiting FA and Dr changes are shown in Fig. 2B and C. The amount of difference in the MCI group compared with that in the CN and SCD groups was approximately 8-15% for FA and 7-10% for Dr (Supplementary Fig. 1).

Among the non-DTI metrics, only OD in cgh and P_0 in fma were significantly different in MCI relative to CN or SCD after the Bonferroni correction. The differences between the SCD and CN groups were no longer significant after the correction.

3.3. Penalized logistic regression and prediction accuracy

The penalized logistic regressions analysis (LASSO) identified three tracts of interest, the parahippocampal cingulum (cgh), posterior thalamic radiation (ptr), and forceps major (fma), as the best classifying predictors of the disease groups (Fig. 3C). In particular, the best predictors for discriminating between SCD and MCI were Dr in the left parahippocampal cingulum, MD in the forceps major, and FA in the left posterior thalamic radiation (Fig. 3A). The area under the receiver operating characteristic curves was 0.83 using all three predictors (bold black line), 0.82 using Dr in the left parahippocampal cingulum and MD in the fornix major (gray line), and 0.80 using Dr in the left parahippocampal cingulum alone (light gray line). The best predictors for discriminating between CN and MCI were FA in the left posterior thalamic radiation and OD in the left parahippocampal cingulum. The areas under the receiver operating characteristic curves were 0.88 using both predictors (bold black line) and 0.82 using FA in the left posterior thalamic radiation alone (gray line) (Fig. 3B). Although each tract is paired with one specific diffusion parameter in the LASSO results, the trend of diffusion changes across the three groups (from CN to MCI) was common in all three tracts of interest, including decreased FA and increased MD, Dr, and OD (Fig. 3D). No predictors were significant for discriminating between CN and SCD. The three tracts of interest that had the best predicting power were used to study associations with the clinical outcome measures described in the next section.

3.4. Clinical associations

We studied associations between the diffusion metrics and the neuropsychological scores within all three groups combined (n = 100), within CN + SCD (n = 78), and within MCI (n = 22) (Supplementary Table 3). In general, worse neuropsychological assessments were consistently associated with lower FA, ICVF, and P_0 and higher MD, Dr, and OD in all three tracts identified with LASSO in Section 3.4 (i.e., the left parahippocampal cingulum, forceps major, and left posterior thalamic radiation). When all three groups were combined, more regressions were significant with mild to moderate correlation coefficients, that is, $r < 0.5$ (as in square root of the adjusted R^2), because of group effects, as expected. Within the combined CN + SCD groups, the diffusion metrics had minimal clinical associations, except that Da had a significant negative association with self-reported CCI ($P < .01$, $r = 0.43$) in the forceps major. The correlations were strongest within the MCI group with all the correlation coefficients (r) ranging from 0.5 to 0.82 with $P < .05$.

Among all neuropsychological scores and diffusion variables, sparse canonical correlation analyses consistently identified RAVLT-IR and Dr as the principal correlative pair. Fig. 4 shows their regression results within all subjects (black line) as well as within the MCI group (red line), where worse verbal memory performance was significantly associated with higher radial diffusivities. Note that while the MCI group had higher correlation coefficients (r) describing the "tightness" or goodness of the fit, it had a lower slope than all the groups combined because of the expected smaller dynamic range of RAVLT-IR scores in MCI.

4. Discussion

White matter alterations in aging individuals with memory complains and deficits were characterized by a series of complementary diffusion metrics derived from nonparametric q-space analysis and parametric analyses with the diffusion tensor and NODDI model. Significantly lower DTI FA, lower P_0, higher radial and MD, and higher fiber orientation dispersion were observed in the cingulum, thalamic radiation, and forceps major of participants with MCI. These tracts of interest also had the highest predictive power to discriminate groups. Dr was significantly associated with cognitive performance, particularly Rey Auditory Verbal Learning Test immediate recall, with the highest association observed in participants with MCI.

Consistent with previous DTI studies [8,11–17], our results demonstrated that subjects with MCI had significantly decreased FA and increased MD and Dr in the white matter. With relatively stable Da, the differences in FA and MD were mostly driven by the increase in Dr, suggesting deterioration in the axonal membrane and/or myelin sheathes [6]. This implication is supported by decreased P_0, a measure of tissue restriction, which is sensitive to myelination in animal and human studies [22–24]. In addition, decreased ICVF and increased OD, a proxy for axonal density and orientation dispersion, respectively, suggested more advanced axonal degeneration and

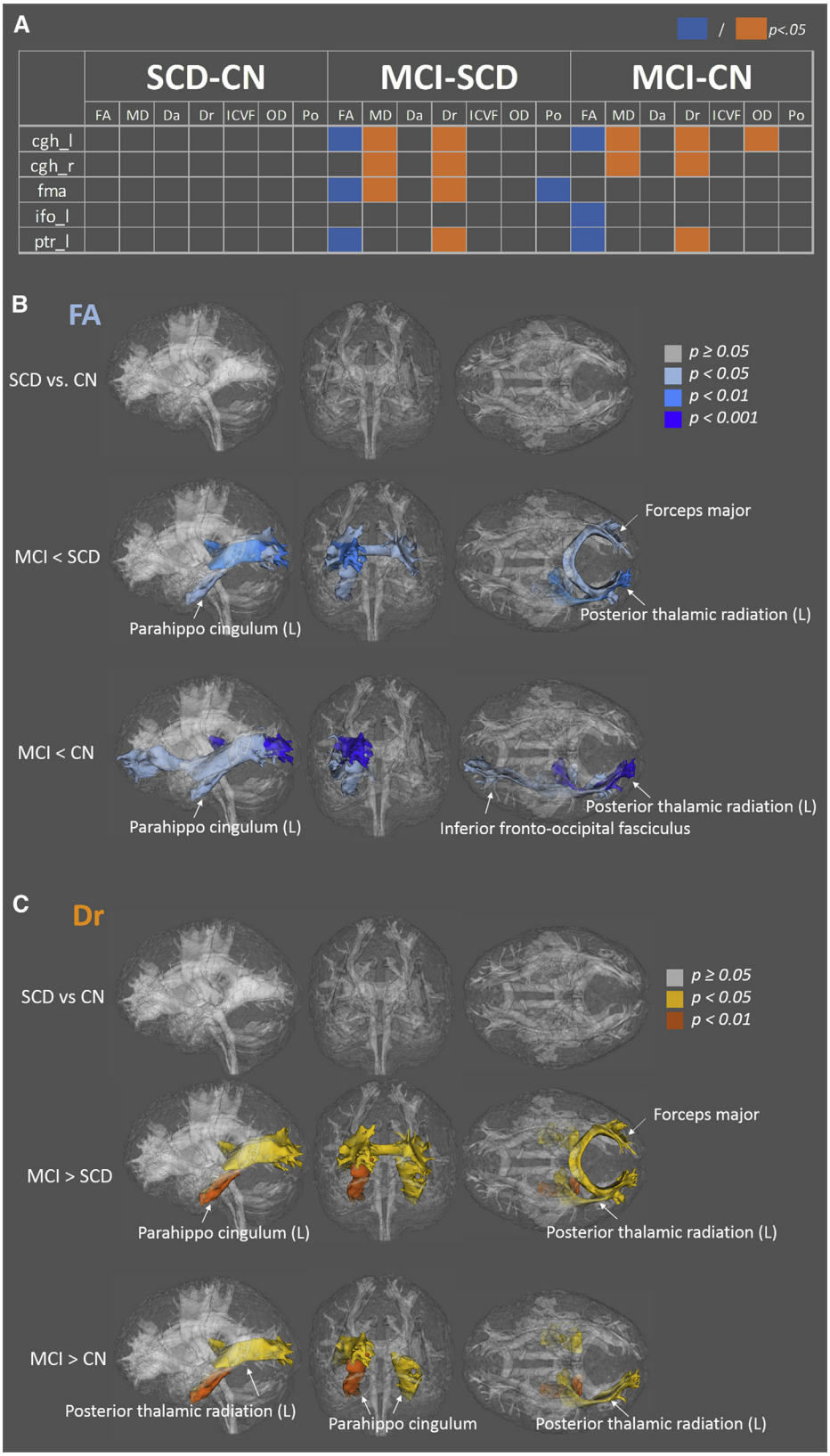

Fig. 2. Tracts exhibiting significant differences after the Bonferroni correction. (A) Tests showing significant differences are highlighted in orange (higher in disease group) or blue (lower in disease group). (B) Tracts exhibiting significant differences in FA, with color labeling indicating different significance levels. Rendered in sagittal (left), coronal (center), and axial (right) views. (C) Tracts showing significant differences in Dr. Abbreviations: SCD, subjective cognitive decline; CN, cognitively normal; MCI, mild cognitive impairment; FA, fractional anisotropy; MD, mean diffusivity; Da, axial diffusivity; Dr, radial diffusivity; ICVF, intra-axonal volume fraction; OD, orientation dispersion; P_0, zero-displacement probability; cgh_l, left parahippocampal cingulum; cgh_r, right parahippocampal cingulum; fma, forceps major; ifo_l, inferior fronto-occipital fasciculi left; ptr_l, left posterior thalamic radiation.

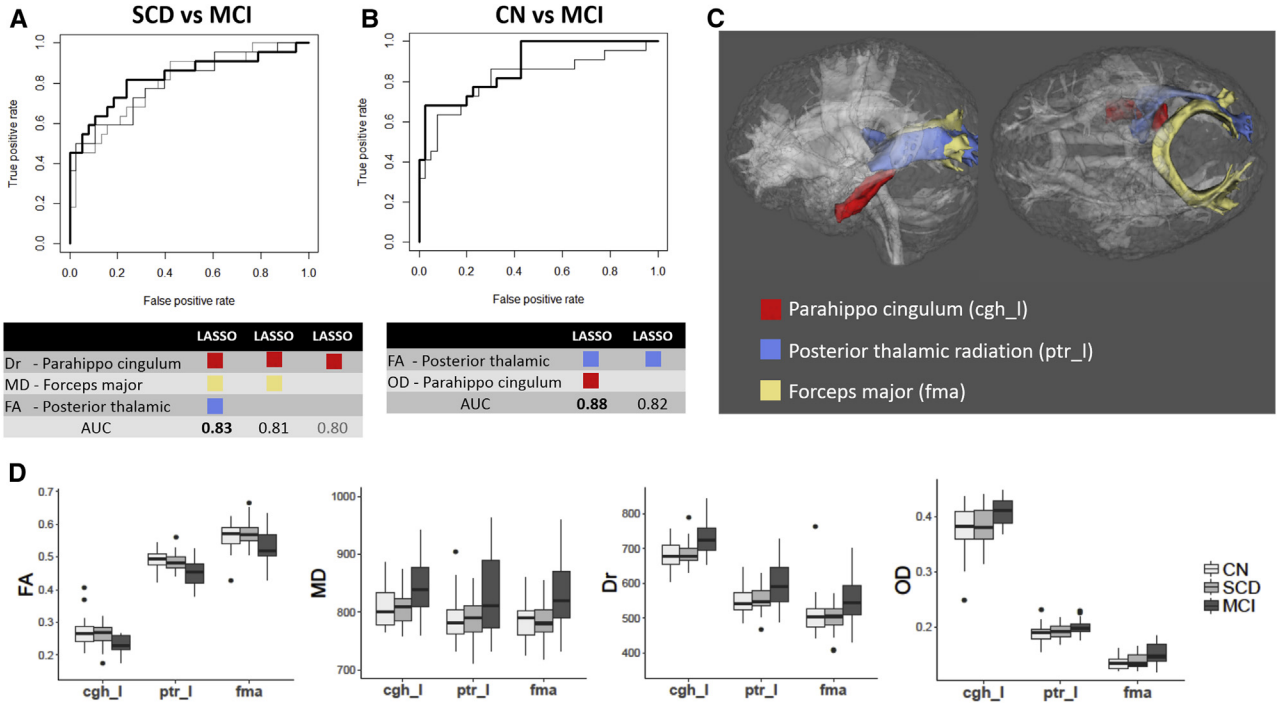

Fig. 3. Best predictors identified by penalized logistic regression (LASSO). (A) The receiver operating characteristic (ROC) curves for each combination of predictors (i.e., diffusion and tract of interest pairs) selected by LASSO for discriminating between SCD and MCI. The best predictors for SCD and MCI were Dr in the left parahippocampal cingulum (cgh_l), MD in the forceps major (fma), and FA in the left posterior thalamic radiation (ptr_l). The area under the ROC curve (AUC) was 0.83 with all three predictors (bold black line), 0.81 with Dr-cgh_l and MD-fma (gray line), and 0.80 with only Dr-cgh_l (light gray line). (B) The ROC curves for each combination of predictors selected by LASSO for discriminating between CN and MCI. The best predictors for CN and MCI were FA-ptr_l and OD-cgh_l. The areas under the ROC curve were 0.88 using both predictors (bold black line) and 0.82 using only FA-ptr_l (gray line). (C) Anatomical locations of the three most sensitive tracts of interest: left parahippocampal cingulum (cgh_l), left posterior thalamic radiation (ptr_l), and forceps major (fma). (D) Boxplots of LASSO-selected diffusion parameters (vertical axes) in the three most sensitive tracts of interest (horizontal axes) for all groups. Abbreviations: LASSO, least absolute shrinkage and selection operator; SCD, subjective cognitive decline; CN, cognitively normal; MCI, mild cognitive impairment; FA, fractional anisotropy; MD, mean diffusivity; Dr, radial diffusivity; OD, orientation dispersion.

loosened axonal bundles [34]. Although the effect size of the NODDI-derived axonal density metric, ICVF, did not survive the adjustment for multiple comparisons, these emerging results warrant further studies with a larger sample size.

The tract-specific studies presented here are different from the tract-based spatial statistical analyses. Tract-based spatial statistical analysis is a voxel-based analysis on DTI-FA–defined white matter skeleton in a standard

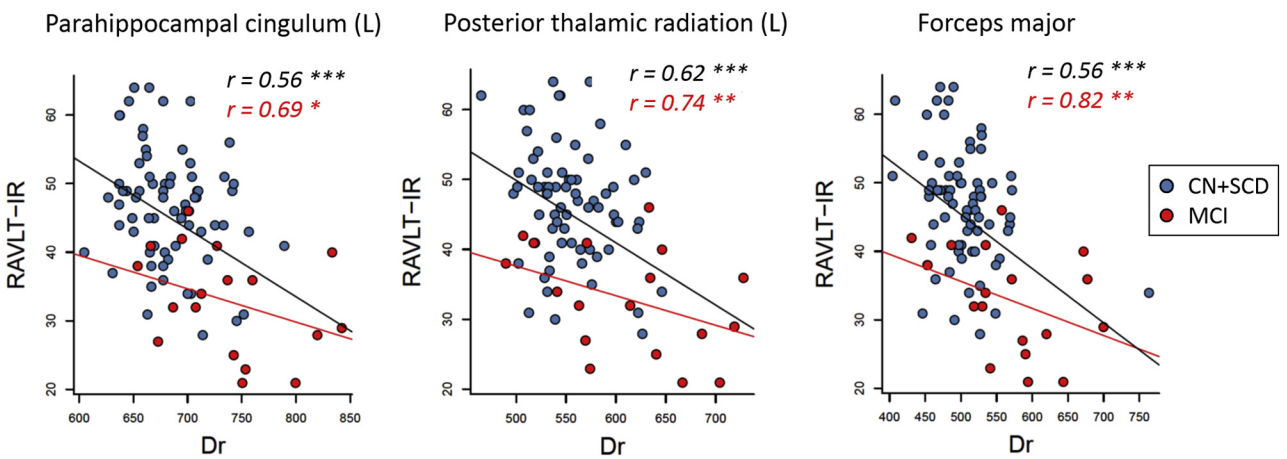

Fig. 4. Linear regression analyses between Rey Auditory Verbal Learning Test immediate recall (RAVLT-IR) and radial diffusivity (Dr) in the left parahippocampal cingulum, posterior thalamic radiation, and forceps major. The correlation coefficient as in goodness of fit (r) is labeled in black for all subjects combined (n = 100, black regression line) and with red for MCI (n = 22, red regression line). Significance level is labeled as: * for $P < .05$, ** for $P < .01$, and *** for $P < .001$. Abbreviations: SCD, subjective cognitive decline; CN, cognitively normal; MCI, mild cognitive impairment.

space. It relies on high-quality registration across subjects, which could be challenging in some cases [51,52]. Alternatively, the tract-specific analyses use tractography to render entire fiber bundles in the subject diffusion space and take account for all the voxels within the fiber bundle.

Previous tract-specific AD studies focused on a single preselected tract, such as the uncinate fasciculus [53,54] and cingulum bundle [14], or on fibers in the limbic system [16,55], whereas few studies have thoroughly investigated whole brain white matter bundles [15,47]. Similar to previous findings, the parahippocampal cingulum exhibited significant sensitivity and predictive accuracy between the three groups. The significant decrease in FA and increase in Dr suggest microstructural disruption in the parahippocampal cingulum in the MCI group. The parahippocampal cingulum bundle is highly related to MCI and AD as it connects the hippocampus to the rest of the brain area [56,57]. Deteriorations in the parahippocampal cingulum are associated with episodic memory in nondementing elderly adults [58] and in those with AD [59].

In addition, we identified two other major fiber bundles, the posterior thalamic radiation and forceps major, that consistently demonstrated significant sensitivity and classification accuracy in both the ANOVA and penalized logistic regression analyses. The posterior thalamic radiation connects the caudal parts of the thalamus with the occipital and parietal lobes, while the forceps major facilitates interhemispheric communication. Although not previously reported in AD studies, the pulvinar nuclei of the caudal thalamus play a role in selective attention, particularly visual attention filtering and focusing [60,61]. Similarly, not previously reported in AD, the microstructures detected by DTI in the forceps major are associated with visuospatial working memory in the developing brain [62].

Overall, the identified fiber bundles are located at the posterior part of the brain, suggesting a posterior-anterior gradient. Such gradients support the Braak staging and recent evidence of spatial distribution of tau deposition across AD stages [63]. Furthermore, these fiber bundles were all significantly associated with auditory verbal learning performance with a trend of higher correlation coefficient in the MCI group (not tested), supporting the earlier hypothesis of accumulating cognitive deficits [64].

Overall, the diffusion measurements in individuals with SCD were intermediate between the CN and MCI groups (Supplementary Fig. 1). Despite the known etiological heterogeneity and modest group sample sizes, we detected emerging signals, although weak at this point, of sensitivity in diffusion metrics for differentiating SCD from CN. Notably, Da in the forceps major and superior longitudinal fasciculus differed significantly between CN and SCD at uncorrected $P < .05$ (Supplementary Fig. 2A). Moreover, Da in the forceps major was also significantly associated with performance in the assessment of perceived cognitive change (i.e., CCI) for the CN and SCD groups (Supplementary Table 3). Future large-sample studies may provide sufficient power to determine the significance of the small effect size between CN and SCD. Owing to the spatial heterogeneity of the initial pathophysiological changes (e.g., varying locations of amyloid-beta–triggered neuronal apoptosis and degeneration [65]), the group-wise analyses, which search for synchronized abnormalities and penalize intersubject variation, may not be efficient for detecting heterogenous subject-specific alterations. Thus, alternatively, subject-specific analytical approaches [66,67] may be more sensitive for detecting subtle microstructural changes in the preclinical stage of AD [68].

In this study, no significant differences between CN and SCD were observed. Widespread, but inconsistent, changes in diffusion metrics in SCD have been reported, with higher MD and Dr [9] and lower MD and Dr [11]. The SCD in these previous studies, however, was categorized differently with significantly decreased AVLT scores [9] or decreased MMSE and RAVLT [11]. In this study, the SCD group was classified more stringently with no significant differences from the CN controls in any objective cognitive assessments (e.g., RAVLT-IR, RAVLT-DR, and MoCA). The term SCD, which has also been variously referred to as cognitive complaints [35], significant memory concern in ADNI [43], and, at times, subjective memory impairment refers to a somewhat heterogeneous early stage, and definitions tend to vary across studies that preceded a recent consensus definition [69] and operational criteria [70].

Limitations of the present study include preclinical cerebrovascular disease affecting white matter, a cross-sectional study design with progression to AD not yet known, modest group sample sizes, a lack of AD subjects as the benchmark, and potentially the choice of the diffusion model. Although NODDI provides a clinically feasible approach with robust nonlinear data fitting for probing axonal density *in vivo*, NODDI estimates may deviate in severe disease conditions where white matter microstructures are highly distorted [71]. We considered the subtle white matter microscopic changes in early stage AD may still satisfy NODDI model assumptions. Alternative options may be to use white matter track integrity based on diffusion kurtosis imaging [19], to model the axons based on composite hindered and restricted model of diffusion (CHARMED) [18], or to measure microscopic anisotropy using spherical tensor encoding [72]. These options, however, require different sets of diffusion constraints, ill-fitted voxels resulting in "black holes" requiring imaging smoothing, many more diffusion encoding directions, or special MRI pulse sequences (non-product sequences).

Acknowledgments

This work was supported by the National Institutes of Health R01 AG053993, P30 AG010133, R01 AG019771, and K01 AG049050 and by the Donors Cure Foundation.

Supplementary Data

Supplementary data related to this article can be found at https://doi.org/10.1016/j.dadm.2019.06.003.

RESEARCH IN CONTEXT

1. Systematic review: The authors reviewed the literature using PubMed. There have been several publications demonstrating the sensitivity of diffusion magnetic resonance imaging in Alzheimer's disease. Most of these publications used diffusion tensor imaging, a sensitive but non–biologically specific imaging technique, on prior selected white matter tracts. These relevant citations are appropriately cited.
2. Interpretation: Our results support existing findings reported in the literature and, most importantly, provide a more comprehensive interpretation of microstructural alterations in the white matter across Alzheimer's disease spectrum using advanced diffusion imaging techniques with parametric compartment analyses and nonparametric q-space analyses.
3. Future directions: Although we found emerging signals in detecting individuals with subjective cognitive decline, future large-sample studies may provide sufficient power to determine the significance of the small effect size. Alternatively, subject-specific analytical approaches may be more sensitive for detecting subtle but heterogenous microstructural changes in this preclinical stage of Alzheimer's disease.

References

[1] Jack CR Jr, Lowe VJ, Weigand SD, Wiste HJ, Senjem ML, Knopman DS, et al., Alzheimer's Disease Neuroimaging Initiative. Serial PIB and MRI in normal, mild cognitive impairment and Alzheimer's disease: implications for sequence of pathological events in Alzheimer's disease. Brain 2009;132:1355–65.

[2] Sperling RA, Aisen PS, Beckett LA, Bennett DA, Craft S, Fagan AM, et al. Toward defining the preclinical stages of Alzheimer's disease: recommendations from the National Institute on Aging-Alzheimer's Association workgroups on diagnostic guidelines for Alzheimer's disease. Alzheimers Dement 2011;7:280–92.

[3] Braak H, Braak E. Neuropathological stageing of Alzheimer-related changes. Acta Neuropathol 1991;82:239–59.

[4] Brun A, Englund E. A white matter disorder in dementia of the Alzheimer type: a pathoanatomical study. Ann Neurol 1986;19:253–62.

[5] Bartzokis G. Alzheimer's disease as homeostatic responses to age-related myelin breakdown. Neurobiol Aging 2011;32:1341–71.

[6] Song SK, Sun SW, Ramsbottom MJ, Chang C, Russell J, Cross AH. Dysmyelination revealed through MRI as increased radial (but unchanged axial) diffusion of water. Neuroimage 2002;17:1429–36.

[7] Amlien IK, Fjell AM. Diffusion tensor imaging of white matter degeneration in Alzheimer's disease and mild cognitive impairment. Neuroscience 2014;276:206–15.

[8] Wang Y, West JD, Flashman LA, Wishart HA, Santulli RB, Rabin LA, et al. Selective changes in white matter integrity in MCI and older adults with cognitive complaints. Biochim Biophys Acta 2012;1822:423–30.

[9] Li XY, Tang ZC, Sun Y, Tian J, Liu ZY, Han Y. White matter degeneration in subjective cognitive decline: a diffusion tensor imaging study. Oncotarget 2016;7:54405–14.

[10] Kiuchi K, Kitamura S, Taoka T, Yasuno F, Tanimura M, Matsuoka K, et al. Gray and white matter changes in subjective cognitive impairment, amnestic mild cognitive impairment and Alzheimer's disease: a voxel-based analysis study. PLoS One 2014;9:e104007.

[11] Selnes P, Fjell AM, Gjerstad L, Bjornerud A, Wallin A, Due-Tonnessen P, et al. White matter imaging changes in subjective and mild cognitive impairment. Alzheimers Dement 2012;8:S112–21.

[12] Nir TM, Jahanshad N, Villalon-Reina JE, Toga AW, Jack CR, Weiner MW, et al. Effectiveness of regional DTI measures in distinguishing Alzheimer's disease, MCI, and normal aging. Neuroimage Clin 2013;3:180–95.

[13] Cardenas VA, Tosun D, Chao LL, Fletcher PT, Joshi S, Weiner MW, et al. Voxel-wise co-analysis of macro- and microstructural brain alteration in mild cognitive impairment and Alzheimer's disease using anatomical and diffusion MRI. J Neuroimaging 2014;24:435–43.

[14] Bozzali M, Giulietti G, Basile B, Serra L, Spano B, Perri R, et al. Damage to the cingulum contributes to Alzheimer's disease pathophysiology by deafferentation mechanism. Hum Brain Mapp 2012;33:1295–308.

[15] Lee SH, Coutu JP, Wilkens P, Yendiki A, Rosas HD, Salat DH, et al. Alzheimer's disease neuroimaging, tract-based analysis of white matter degeneration in Alzheimer's disease. Neuroscience 2015;301:79–89.

[16] Pievani M, Agosta F, Pagani E, Canu E, Sala S, Absinta M, et al. Assessment of white matter tract damage in mild cognitive impairment and Alzheimer's disease. Hum Brain Mapp 2010;31:1862–75.

[17] Scrascia F, Curcio G, Ursini F, Trotta L, Quintiliani L, Migliore S, et al. Relationship among diffusion tensor imaging, EEG activity, and cognitive status in mild cognitive impairment and Alzheimer's disease patients. J Alzheimers Dis 2014;38:939–50.

[18] Assaf Y, Basser PJ. Composite hindered and restricted model of diffusion (CHARMED) MR imaging of the human brain. Neuroimage 2005;27:48–58.

[19] Fieremans E, Jensen JH, Helpern JA. White matter characterization with diffusional kurtosis imaging. Neuroimage 2011;58:177–88.

[20] Zhang H, Schneider T, Wheeler-Kingshott CA, Alexander DC. NODDI: practical in vivo neurite orientation dispersion and density imaging of the human brain. Neuroimage 2012;61:1000–16.

[21] Wang Y, Sun P, Wang Q, Trinkaus K, Schmidt RE, Naismith RT, et al. Differentiation and quantification of inflammation, demyelination and axon injury or loss in multiple sclerosis. Brain 2015;138:1223–38.

[22] Wu YC, Field AS, Duncan ID, Samsonov AA, Kondo Y, Tudorascu D, et al. High b-value and diffusion tensor imaging in a canine model of dysmyelination and brain maturation. Neuroimage 2011;58:829–37.

[23] Biton IE, Duncan ID, Cohen Y. High b-value q-space diffusion MRI in myelin-deficient rat spinal cords. Magn Reson Imaging 2006;24:161–6.

[24] Assaf Y, Chapman J, Ben-Bashat D, Hendler T, Segev Y, Korczyn AD, et al. White matter changes in multiple sclerosis: correlation of q-space diffusion MRI and 1H MRS. Magn Reson Imaging 2005;23:703–10.

[25] Kodiweera C, Alexander AL, Harezlak J, Mcallister TW, Wu YC. Age effects and sex differences in human brain white matter of young to middle-aged adults: A DTI, NODDI, and q-space study. Neuroimage 2016;128:180–92.

[26] Stanisz GJ, Szafer A, Wright GA, Henkelman RM. An analytical model of restricted diffusion in bovine optic nerve. Magn Reson Med 1997;37:103–11.
[27] Jespersen SN, Kroenke CD, Ostergaard L, Ackerman JJ, Yablonskiy DA. Modeling dendrite density from magnetic resonance diffusion measurements. Neuroimage 2007;34:1473–86.
[28] Sepehrband F, Clark KA, Ullmann JF, Kurniawan ND, Leanage G, Reutens DC, et al. Brain tissue compartment density estimated using diffusion-weighted MRI yields tissue parameters consistent with histology. Hum Brain Mapp 2015;36:3687–702.
[29] Colgan N, Siow B, O'callaghan JM, Harrison IF, Wells JA, Holmes HE, et al. Application of neurite orientation dispersion and density imaging (NODDI) to a tau pathology model of Alzheimer's disease. Neuroimage 2015;125:739–44.
[30] Billiet T, Vandenbulcke M, Madler B, Peeters R, Dhollander T, Zhang H, et al. Age-related microstructural differences quantified using myelin water imaging and advanced diffusion MRI. Neurobiol Aging 2015;36:2107–21.
[31] Nazeri A, Chakravarty MM, Rotenberg DJ, Rajji TK, Rathi Y, Michailovich OV, et al. Functional consequences of neurite orientation dispersion and density in humans across the adult lifespan. J Neurosci 2015;35:1753–62.
[32] Merluzzi AP, Dean DC 3rd, Adluru N, Suryawanshi GS, Okonkwo OC, Oh JM, et al. Age-dependent differences in brain tissue microstructure assessed with neurite orientation dispersion and density imaging. Neurobiol Aging 2016;43:79–88.
[33] Cox SR, Ritchie SJ, Tucker-Drob EM, Liewald DC, Hagenaars SP, Davies G, et al. Ageing and brain white matter structure in 3,513 UK Biobank participants. Nat Commun 2016;7:13629.
[34] Slattery CF, Zhang J, Paterson RW, Foulkes AJM, Carton A, Macpherson K, et al. ApoE influences regional white-matter axonal density loss in Alzheimer's disease. Neurobiol Aging 2017;57:8–17.
[35] Saykin AJ, Wishart HA, Rabin LA, Santulli RB, Flashman LA, West JD, et al. Older adults with cognitive complaints show brain atrophy similar to that of amnestic MCI. Neurology 2006;67:834–42.
[36] Rattanabannakit C, Risacher SL, Gao S, Lane KA, Brown SA, Mcdonald BC, et al. The Cognitive Change Index as a measure of self and informant perception of cognitive decline: relation to neuropsychological tests. J Alzheimers Dis 2016;51:1145–55.
[37] De Groot M, Vernooij MW, Klein S, Ikram MA, Vos FM, Smith SM, et al. Improving alignment in tract-based spatial statistics: evaluation and optimization of image registration. Neuroimage 2013;76:400–11.
[38] Weintraub S, Besser L, Dodge HH, Teylan M, Ferris S, Goldstein FC, et al. Version 3 of the Alzheimer disease centers' neuropsychological test battery in the Uniform Data Set (UDS). Alzheimer Dis Assoc Disord 2018;32:10–7.
[39] Nasreddine ZS, Phillips NA, Bedirian V, Charbonneau S, Whitehead V, Collin I, et al. The Montreal Cognitive Assessment, MoCA: a brief screening tool for mild cognitive impairment. J Am Geriatr Soc 2005;53:695–9.
[40] O'bryant SE, Waring SC, Cullum CM, Hall J, Lacritz L, Massman PJ, et al., Texas Alzheimer's Research Consortium. Staging dementia using clinical dementia rating scale sum of boxes scores: a Texas Alzheimer's research consortium study. Arch Neurol 2008;65:1091–5.
[41] Marc LG, Raue PJ, Bruce ML. Screening performance of the 15-item geriatric depression scale in a diverse elderly home care population. Am J Geriatr Psychiatry 2008;16:914–21.
[42] Albert MS, Dekosky ST, Dickson D, Dubois B, Feldman HH, Fox NC, et al. The diagnosis of mild cognitive impairment due to Alzheimer's disease: recommendations from the National Institute on Aging-Alzheimer's Association workgroups on diagnostic guidelines for Alzheimer's disease. Alzheimers Dement 2011;7:270–9.
[43] Risacher SL, Kim S, Nho K, Foroud T, Shen L, Petersen RC, et al., Alzheimer's Disease Neuroimaging Initiative. APOE effect on Alzheimer's disease biomarkers in older adults with significant memory concern. Alzheimers Dement 2015;11:1417–29.
[44] Wu YC, Alexander AL. Hybrid diffusion imaging. Neuroimage 2007;36:617–29.
[45] Manjon JV, Coupe P, Concha L, Buades A, Collins DL, Robles M. Diffusion weighted image denoising using overcomplete local PCA. PLoS One 2013;8:e73021.
[46] Daducci A, Canales-Rodriguez EJ, Zhang H, Dyrby TB, Alexander DC, Thiran JP. Accelerated Microstructure Imaging via Convex Optimization (AMICO) from diffusion MRI data. Neuroimage 2015;105:32–44.
[47] Douaud G, Jbabdi S, Behrens TE, Menke RA, Gass A, Monsch AU, et al. DTI measures in crossing-fibre areas: increased diffusion anisotropy reveals early white matter alteration in MCI and mild Alzheimer's disease. Neuroimage 2011;55:880–90.
[48] Behrens TE, Berg HJ, Jbabdi S, Rushworth MF, Woolrich MW. Probabilistic diffusion tractography with multiple fibre orientations: What can we gain? Neuroimage 2007;34:144–55.
[49] Wakana S, Jiang H, Nagae-Poetscher LM, Van Zijl PC, Mori S. Fiber tract-based atlas of human white matter anatomy. Radiology 2004;230:77–87.
[50] Tibshirani R. Regression Shrinkage and Selection via the Lasso. J R Stat Soc Ser B 1996;58:267–88.
[51] Zalesky A. Moderating registration misalignment in voxelwise comparisons of DTI data: a performance evaluation of skeleton projection. Magn Reson Imaging 2011;29:111–25.
[52] Bach M, Laun FB, Leemans A, Tax CM, Biessels GJ, Stieltjes B, et al. Methodological considerations on tract-based spatial statistics (TBSS). Neuroimage 2014;100:358–69.
[53] Serra L, Cercignani M, Basile B, Spano B, Perri R, Fadda L, et al. White matter damage along the uncinate fasciculus contributes to cognitive decline in AD and DLB. Curr Alzheimer Res 2012;9:326–33.
[54] Morikawa M, Kiuchi K, Taoka T, Nagauchi K, Kichikawa K, Kishimoto T. Uncinate fasciculus-correlated cognition in Alzheimer's disease: a diffusion tensor imaging study by tractography. Psychogeriatrics 2010;10:15–20.
[55] Ringman JM, O'neill J, Geschwind D, Medina L, Apostolova LG, Rodriguez Y, et al. Diffusion tensor imaging in preclinical and presymptomatic carriers of familial Alzheimer's disease mutations. Brain 2007;130:1767–76.
[56] Bubb EJ, Metzler-Baddeley C, Aggleton JP. The cingulum bundle: Anatomy, function, and dysfunction. Neurosci Biobehav Rev 2018;92:104–27.
[57] Yu J, Lam CLM, Lee TMC. White matter microstructural abnormalities in amnestic mild cognitive impairment: A meta-analysis of whole-brain and ROI-based studies. Neurosci Biobehav Rev 2017;83:405–16.
[58] Ezzati A, Katz MJ, Lipton ML, Zimmerman ME, Lipton RB. Hippocampal volume and cingulum bundle fractional anisotropy are independently associated with verbal memory in older adults. Brain Imaging Behav 2016;10:652–9.
[59] Kantarci K, Murray ME, Schwarz CG, Reid RI, Przybelski SA, Lesnick T, et al. White-matter integrity on DTI and the pathologic staging of Alzheimer's disease. Neurobiol Aging 2017;56:172–9.
[60] Grieve KL, Acuna C, Cudeiro J. The primate pulvinar nuclei: vision and action. Trends Neurosci 2000;23:35–9.
[61] Laberge D, Buchsbaum MS. Positron emission tomographic measurements of pulvinar activity during an attention task. J Neurosci 1990;10:613–9.
[62] Krogsrud SK, Fjell AM, Tamnes CK, Grydeland H, Due-Tonnessen P, Bjornerud A, et al. Development of white matter microstructure in relation to verbal and visuospatial working memory-A longitudinal study. PLoS One 2018;13:e0195540.
[63] Scholl M, Lockhart SN, Schonhaut DR, O'neil JP, Janabi M, Ossenkoppele R, et al. PET imaging of tau deposition in the aging human brain. Neuron 2016;89:971–82.

[64] Nakata Y, Sato N, Nemoto K, Abe O, Shikakura S, Arima K, et al. Diffusion abnormality in the posterior cingulum and hippocampal volume: correlation with disease progression in Alzheimer's disease. Magn Reson Imaging 2009;27:347–54.

[65] Stefaniak J, O'brien J. Imaging of neuroinflammation in dementia: a review. J Neurol Neurosurg Psychiatry 2016;87:21–8.

[66] White T, Schmidt M, Karatekin C. White matter 'potholes' in early-onset schizophrenia: a new approach to evaluate white matter microstructure using diffusion tensor imaging. Psychiatry Res 2009;174:110–5.

[67] Mayer AR, Bedrick EJ, Ling JM, Toulouse T, Dodd A. Methods for identifying subject-specific abnormalities in neuroimaging data. Hum Brain Mapp 2014;35:5457–70.

[68] Elsaid NMH, Wen Q, Mustafi SM, Risacher SL, Farlow MR, Apostolova LG, et al, Alterations in White-Matter Diffusion Metrics in Preclinical Alzheimer's Disease: A Subject-Specific Analysis. in Alzheimer's Association International Conference (AAIC) 2018. Chicago, USA.

[69] Jessen F, Amariglio RE, Van Boxtel M, Breteler M, Ceccaldi M, Chetelat G, et al., Subjective Cognitive Decline Initiative Working Group. A conceptual framework for research on subjective cognitive decline in preclinical Alzheimer's disease. Alzheimers Dement 2014;10:844–52.

[70] Molinuevo JL, Rabin LA, Amariglio R, Buckley R, Dubois B, Ellis KA, et al., Subjective Cognitive Decline Initiative Working Group. Implementation of subjective cognitive decline criteria in research studies. Alzheimers Dement 2017;13:296–311.

[71] Guerrero JM, Adluru N, Kecskemeti SR, Davidson RJ, Alexander AL. Investigating the effects of intrinsic diffusivity on neurite orientation dispersion and density imaging (NODDI). Singapore: ISMRM; 2016.

[72] Lawrenz M, Brassen S, Finsterbusch J. Microscopic diffusion anisotropy in the human brain: Age-related changes. Neuroimage 2016; 141:313–25.